Journal of Inorganic and Organometallic Polymers and Materials
https://doi.org/10.1007/s10904-023-02652-6

RESEARCH

Remarkable High Adsorption of Methylene Blue Dye from Aqueous Solutions Using Facilely Synthesized $MgFe_2O_4$ Nanoparticles

Asma S. Al-Wasidi[1] · Faisal K. Algethami[2] · Fawaz A. Saad[3] · Ehab A. Abdelrahman[2,4]

Received: 20 March 2023 / Accepted: 10 April 2023

Abstract
In this work, the efficacy of $MgFe_2O_4$ nanoparticles as an adsorbent for the removal of the toxic methylene blue dye from aqueous media under ultrasonication was evaluated. The $MgFe_2O_4$ nanoparticles displayed a BET surface area of 62.29 m^2/g and a pore volume of 0.1523 cc/g. In addition, the mean pore diameter is 4.62 nm, which verifies the mesoporous character of the $MgFe_2O_4$ nanoparticles. Besides, the average crystallite size is 15.86 nm. The FE-SEM image of $MgFe_2O_4$ nanoparticles showed the presence of spherical particles with a mean grain size of 0.21 µm. Also, the TEM image of $MgFe_2O_4$ nanoparticles showed the presence of polyhedral particles with a mean diameter of 42.50 nm. Besides, the ultrasonication aids in achieving equilibrium in a shorter contact time than other conventional adsorption procedures such as stirring and shaking due to the enhanced mass transfer. The maximum adsorption capacity of $MgFe_2O_4$ nanoparticles toward methylene blue dye is 537.63 mg/g. Adsorption of methylene blue dye using $MgFe_2O_4$ nanoparticles fits well with the Langmuir equilibrium isotherm as well as the pseudo-second-order kinetic model.

Keywords Adsorption · Nanoparticles · Methylene blue dye · Ultrasonication

1 Introduction

Based on water consumption, the textile industry is second only to the sector of agricultural depending on the quantity of water required for production. The dying route in the textile manufacturing requires more than fifty percent of the entire water consumption and produces the majority of wastes with unfixed dyes as the main component [1]. Synthetic dyes are widely employed in the manufacture of printing inks, pharmaceuticals, textiles, plastics, food, cosmetics, paper, and photographic materials due to their great coloring capability and very low cost [4, 5]. The issue of discharging colored effluent from textile industries has a detrimental impact on aquatic ecosystems and other forms of life. Several organic dyes and their breakdown compounds are considered mutagenic and toxic to humans, causing respiratory diseases, dermal dysfunction, allergic reactions in the eyes, irritation of the mucous membranes and upper respiratory tract, etc. [6–8]. The presence of minor quantities of dyes in water severely degrades its chemical and physical properties. Dyes impede photosynthesis activity and light diffusion capacity, enhancing oxygen deficiency, and limiting beneficial downstream usages such as recreation, irrigation, and water supply [9]. Methylene blue dye is a cationic thiazine dye. Methylene blue dye is widely utilized in the silk, paper, leather, acrylic, and food industries. As methylene blue dye was recognized for its carcinogenic properties on mammals and fish kinds, including humans, it is regarded as a dangerous, cytotoxic, and tumor-promoting compound. In addition, it can irritate the gastrointestinal and respiratory tracts and cause skin problems such as rashes, edema, etc. [10, 11]. Hence, methylene blue dye was chosen in this work to test the adsorption. Adsorption is one of the quickest and most effective dye removal techniques currently in use in comparison to other methods such as

✉ Ehab A. Abdelrahman
EAAAhmed@imamu.edu.sa; dr.ehabsaleh@yahoo.com

[1] Department of Chemistry, College of Science, Princess Nourah bint Abdulrahman University, P.O. Box 84428, Riyadh 11671, Saudi Arabia

[2] Department of Chemistry, College of Science, Imam Mohammad Ibn Saud Islamic University (IMSIU), Riyadh 11623, Saudi Arabia

[3] Department of Chemistry, Faculty of Applied Sciences, Umm Al-Qura University, Makkah 21955, Saudi Arabia

[4] Chemistry Department, Faculty of Science, Benha University, Benha 13518, Egypt

Published online: 19 April 2023

photocatalytic degradation and electrocoagulation [12–15]. For wastewater remediation, conventional adsorbents such as zeolites, biochars, activated carbon, MgO, magnetic polyacrylonitrile/graphene oxide, ferrous oxalate, Fe_2O_3/SnO_2, and MgO/Fe_2O_3 have been extensively studied [16–22]. But, most of them have disadvantages, such as a long reaction time, limited adsorption capacity, the problem of removing remaining slurry, high operational costs, and production. [23–25]. Thus, novel adsorbents with greater dye removal efficiency, low cost, and high stability are required. Recent advances in nanotechnology have made it possible to manufacture mechanically stable, highly effective, and low-cost adsorbents for efficient wastewater treatment. Spinel ferrite nanoparticles have a greater uptake capability and quicker uptake kinetics than conventional adsorbents. This is because of their great BET surface area in addition to the presence of effective groups on the surface, which facilitate a strong interaction with contaminants such as heavy metal ions and dye molecules [26–28]. $MgFe_2O_4$ is considered a famous cubic ferrite with octahedral and tetrahedral cationic positions occupied by Fe^{3+} and Mg^{2+}, respectively. In addition, $MgFe_2O_4$ is cost-effective, non-toxic, has high thermal stability, is easily separated due to its magnetic property, and does not contribute to secondary pollution. Due to its insoluble character and great affinity for certain environmental pollutants in effluents, it has become an excellent adsorbent for wastewater treatment [29, 30]. Recently, ultrasonication has been used primarily to accelerate chemical reactions by activating acoustic cavitation. Mechanical motivation eliminates the attractive forces between liquid phase molecules during the applied cavitation process. The process of acoustic cavitation includes the creation, growth, and disintegration of minute gas bubbles, and hence this resulting in the production of enormous amounts of energy at a specific location. Cavitation induces convection in solution by means of microturbulence, microjetting, microstreaming, and waves of acoustic. Ultrasonication accelerates the transfer of mass via decreasing the resistance of diffusion and also by severing adsorbate-adsorbent affinities [31, 32]. Therefore, ultrasonication aids in achieving equilibrium in a shorter contact time than other conventional adsorption procedures. In general, metal ferrites are recognized as highly effective for the adsorption of dyes from highly alkaline or highly acidic solutions, though they need a prolonged contact time to attain equilibrium. As the removal of treated industrial waste with a highly alkaline or acidic character can harm the environment, any treatment procedure including highly alkaline or highly acidic solutions can make the procedure more expensive and difficult than its great contaminant removal efficacy. Consequently, the novelty in this work comes through the use of the pechini sol-gel method for the simple and low-cost synthesis of $MgFe_2O_4$ nanoparticles with small size and high surface area. In addition, in comparison with other adsorbents in the literature, the novelty in this work comes through the remarkably high adsorption of methylene blue dye from aqueous solutions using $MgFe_2O_4$ nanoparticles under the effect of ultrasonication. This could make this ultrasonication methylene blue dye adsorption onto $MgFe_2O_4$ nanoparticles suitable for water treatment. Ultrasonication has primarily been utilized to speed up chemical reactions by activating acoustic cavitation. Ultrasonication helps achieve equilibrium in a shorter contact time than other conventional adsorption techniques. In the methodical tests on methylene blue dye adsorption, the effects of various operating parameters, such as pH, time, dose, and concentration, were examined. The pseudo-first-order, pseudo-second-order, Langmuir, and Freundlich equations were applied to determine the mechanism of adsorption of methylene blue dye using $MgFe_2O_4$ nanoparticles. In addition, the efficiency of adsorption under ultrasonication was compared to that of shaking and stirring techniques when $MgFe_2O_4$ nanoparticles were employed for the disposal of methylene blue dye.

2 Experimental

2.1 Chemicals

Magnesium nitrate hexahydrate ($Mg(NO_3)_2.6H_2O$), sodium hydroxide (NaOH), iron(III) nitrate nonahydrate ($Fe(NO_3)_3.9H_2O$), tartaric acid ($C_4H_6O_6$), methylene blue dye ($C_{16}H_{18}N_3SCl$), ethylene glycol ($C_2H_6O_2$), and hydrochloric acid (HCl) were of analytical grade, obtained from the Merck company, and used without refining.

2.2 Synthesis of $MgFe_2O_4$Nanoparticles Using Pechini Sol Gel Method

2.10 g of $Mg(NO_3)_2.6H_2O$ was dissolved in 60 mL of distilled water. After that, 6.62 g of $Fe(NO_3)_3.9H_2O$ was dissolved in 60 mL of distilled water. The above two solutions were mixed with each other and then magnetically stirred for 30 min. In addition, the tartaric acid solution, which was prepared by dissolving 6.15 g of tartaric acid in 75 mL of distilled water, was added then the mixture was magnetically stirred for 30 min. Additionally, 10 mL of ethylene glycol was added from a burette then the mixture was magnetically stirred at 160 °C till dryness. Finally, the produced powder was calcined at 550 °C for 4 h.

2.3 Characterization

Using a Brucker D8 advanced X-ray diffractometer, the X-ray diffraction pattern (XRD) of $MgFe_2O_4$ nanoparticles was obtained. A field emission scanning electron microscope (FE-SEM, Model JSM-IT800 Schottky) connected by an energy dispersive X-ray (EDX) unit was utilized to examine the surface morphology and chemical composition of $MgFe_2O_4$ nanoparticles. The TEM image of $MgFe_2O_4$ nanoparticles was captured by the transmission electron microscope (TEM, Talos F200iS). Using a BET surface area analyzer (Quantachrome, TouchWin), the BET surface area as well as pore characteristics of $MgFe_2O_4$ nanoparticles were estimated. Fourier transform infrared spectroscopy (FT-IR, VERTEX 70v, Bruker) was employed to investigate the functional chemical groups on the $MgFe_2O_4$ nanoparticles.

2.4 Adsorption of Methylene Blue Dye from Aqueous Media

Using the batch approach, adsorption experiments were conducted under ultrasonication at room temperature. In this regard, a predetermined quantity of $MgFe_2O_4$ nanoparticles was mixed with the solution of methylene blue dye, followed by a specific duration of ultrasonication using an ultrasonic reactor (Hielscher, UP200HT, 200 W, 26 kHz). After ultrasonication, the $MgFe_2O_4$ nanoparticles were separated using an external magnetic field, and the methylene blue dye concentration in the supernatant liquid was determined using a UV–Vis spectrophotometer (Shimadzu UV-1650) at the maximum wavelength of the methylene blue dye ($\lambda_{max} = 662$ nm). The methylene blue dye adsorption efficacy (% R) and the uptake capability of $MgFe_2O_4$ nanoparticles (Q, mg/g) were determined using equations (1) and (2), respectively.

$$\% R = \frac{C_o - C_e}{C_o} \times 100 \tag{1}$$

$$Q = \left(C_o - C_e\right) \times \frac{V}{M} \tag{2}$$

In the preceding equations, C_o and C_e represent the initial and equilibrium methylene blue dye concentrations (mg/L), respectively. The parameters 'M' and 'V' represent the quantity of $MgFe_2O_4$ nanoparticles (g) and the volume of methylene blue dye solution (L), respectively. The effect of solution pH on methylene blue dye adsorption by $MgFe_2O_4$ nanoparticles was investigated by modulating the pH from 2 to 10 with an initial methylene blue dye concentration of 300 mg/L, a methylene blue dye volume of 100 mL, an ultrasonication time of 60 min, and an adsorbent dose of 0.05 g. Analogously, the effect of ultrasonication time on the removal efficacy of methylene blue dye by $MgFe_2O_4$ nanoparticles was investigated by modulating the ultrasonication time from 5 min to 35 min with an initial methylene blue dye concentration of 300 mg/L, a methylene blue dye volume of 100 mL, a solution pH of 8, and an adsorbent dose of 0.05 g. In addition, the pseudo-first-order (Eq. 3) and pseudo-second-order (Eq. 4) kinetic models, were used to linearly fit the experimental data of the effect of time on methylene blue dye adsorption using $MgFe_2O_4$ nanoparticles [33].

$$\log\left(Q_e - Q_t\right) = logQ_e - \frac{k_1}{2.303}t \tag{3}$$

$$\frac{t}{Q_t} = \frac{1}{k_2 Q_e^2} + \frac{1}{Q_e}t \tag{4}$$

where, Q_t is the amount of methylene blue dye adsorbed at time t (mg/g), Q_e is the quantity of methylene blue dye adsorbed at equilibrium (mg/g), k_1 is the pseudo-first-order rate constant (1/min), and k_2 is the pseudo-second-order rate constant (g/mg.min). The effect of adsorbent dose on the removal efficacy of methylene blue dye by $MgFe_2O_4$ nanoparticles was examined using adsorbent doses in the range 0.0125—0.20 g, where the initial methylene blue dye concentration, solution pH, methylene blue dye volume, and ultrasonication time equal 300 mg/L, 8, 100 mL, and 25 min, respectively. The effect of methylene blue dye concentration on the removal efficacy of methylene blue dye using $MgFe_2O_4$ nanoparticles was examined using concentrations ranging from 200 to 400 mg/L, with methylene blue dye volume, ultrasonication time, and solution pH of 100 mL, 25 min, and 8, respectively. In addition, the Langmuir (Eq. 5) and Freundlich (Eq. 6) equilibrium isotherms, were exploited to linearly fit the experimental data of effect of concentration on methylene blue dye adsorption using $MgFe_2O_4$ nanoparticles [33].

$$\frac{C_e}{Q_e} = \frac{1}{k_L Q_{max}} + \frac{C_e}{Q_{max}} \tag{5}$$

$$lnQ_e = lnk_F + \frac{1}{z}lnC_e \tag{6}$$

where, 1/z is the heterogeneity constant whereas k_L is the equilibrium constant of the Langmuir isotherm (L/mg). In addition, k_F is the equilibrium constant of the Freundlich isotherm $(mg/g)(L/mg)^{1/n}$ whereas Q_{max} is the maximum uptake capability of the Langmuir isotherm (mg/g). Eq. 7 can be employed to determine the Q_{max} using the Freundlich equilibrium isotherm [33].

$$Q_{max} = k_F\left(C_o^{1/n}\right) \tag{7}$$

3 Results and Discussion

3.1 Characterization of $MgFe_2O_4$ Nanoparticles

Pechini sol–gel method is based on the ability of α-hydroxycarboxylic organic acids such as tartaric acid to form strong chelates with several metal cations such as Mg(II) and Fe(III). After the addition of a polyhydroxylic alcohol such as ethylene glycol to this mixture, it is heated and the chelate is converted into a polymer with a homogeneous distribution of metal cations. Hence, in our work, the XRD pattern of this polymer contains a broad band at 2θ=32° and does not contain sharp crystalline diffraction peaks due to the amorphous nature as shown in Fig. 1.

Finally, the organic part is successively destroyed via calcination at 550 °C, thus forming reactive crystalline metal oxides (i.e. $MgFe_2O_4$ nanoparticles) [34–36]. The XRD pattern of $MgFe_2O_4$ nanoparticles is depicted in Fig. 2A. The obtained diffraction peaks at 2θ= 30.16°, 35.61°, 43.14°, 53.31°, 57.57°, and 63.81° correspond to the (220), (311), (400), (422), (511), and (440) miller planes of the $MgFe_2O_4$ nanoparticles, respectively, as clarified from JCPDS No. 881935. The mean crystallite size of the $MgFe_2O_4$ nanoparticles is 15.86 nm. The EDX pattern of $MgFe_2O_4$ nanoparticles is depicted in Fig. 2B. The results confirmed that the $MgFe_2O_4$ nanoparticles consisted of Mg, Fe, and O with weight percentages equal to 11.56, 62.25, and 26.19%, respectively.

Figure 3A depicts the FE-SEM image of $MgFe_2O_4$ nanoparticles, which suggests the presence of spherical particles with a mean grain size of 0.21 µm. Also, Fig. 3B depicts the TEM image of $MgFe_2O_4$ nanoparticles, which suggests the presence of polyhedral particles with a mean

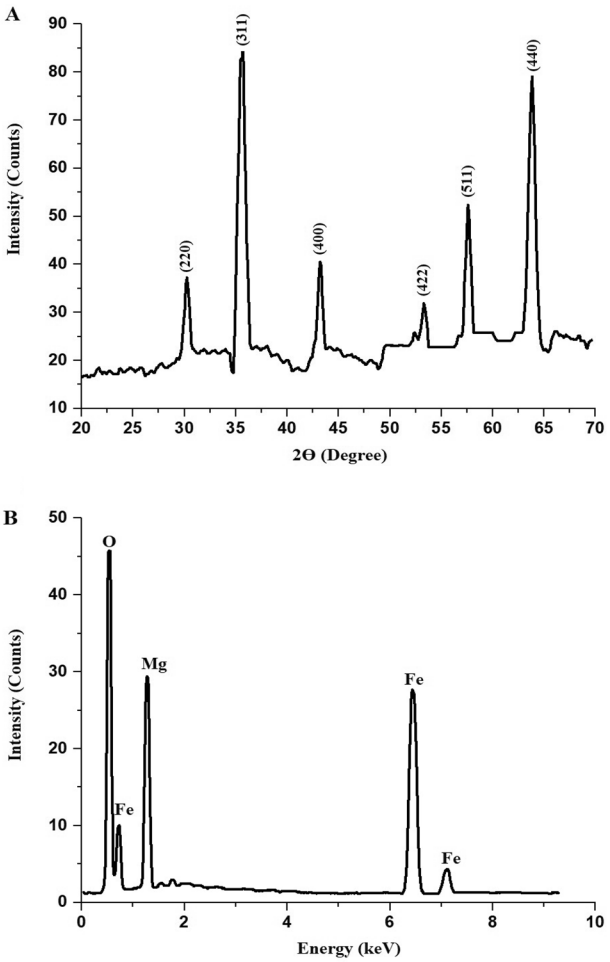

Fig. 2 The XRD (**A**) and EDX (**B**) patterns of the $MgFe_2O_4$ nanoparticles

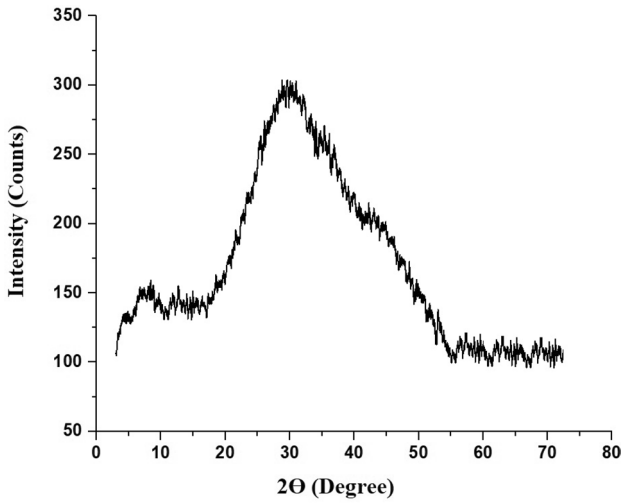

Fig. 1 The XRD pattern of the sample before calcination

diameter of 42.50 nm. In addition, the discrepancy between the XRD and TEM results is due to the agglomeration of particles.

Figure 4 shows the FT-IR spectrum of $MgFe_2O_4$ nanoparticles. Significant peaks at 435 and 595 cm^{-1} correspond to the stretching vibration of Mg–O or Fe–O octahedral and tetrahedral groups, respectively. The other two significant peaks centered at 1492 and 3453 cm^{-1} represent the bending and stretching vibrations of O–H, respectively [37].

The adsorption/desorption isotherm represented in Fig. 5A corresponds to the IV type isotherm, which reveals the mesoporous character of $MgFe_2O_4$ nanoparticles [38]. Also, the pore size distribution curve is shown in Fig. 5B.

The $MgFe_2O_4$ nanoparticles displayed a BET surface area of 62.29 m^2/g and a pore volume of 0.1523 cc/g. In addition, the mean pore diameter is 4.62 nm, which confirms the mesoporous character of the $MgFe_2O_4$ nanoparticles.

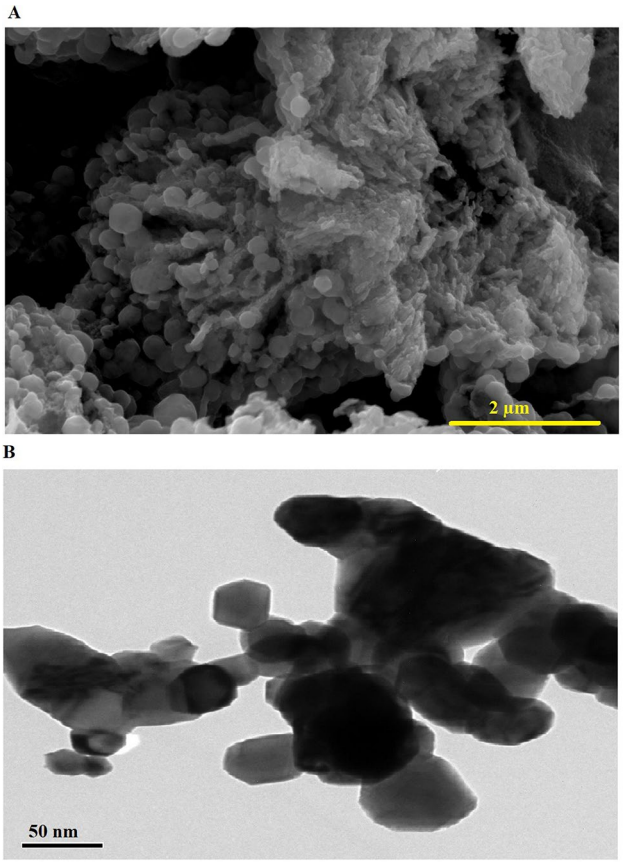

Fig. 3 The FE-SEM (**A**) and TEM (**B**) images of the $MgFe_2O_4$ nanoparticles

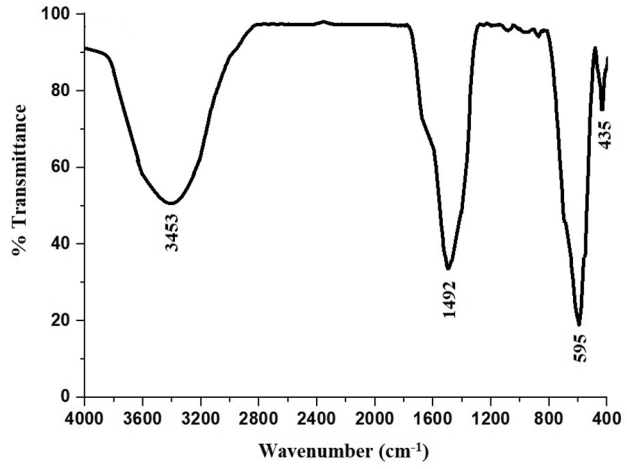

Fig. 4 The FT-IR spectrum of $MgFe_2O_4$ nanoparticles

3.2 Adsorption of Methylene Blue Dye from Aqueous Solutions

3.2.1 pH Study

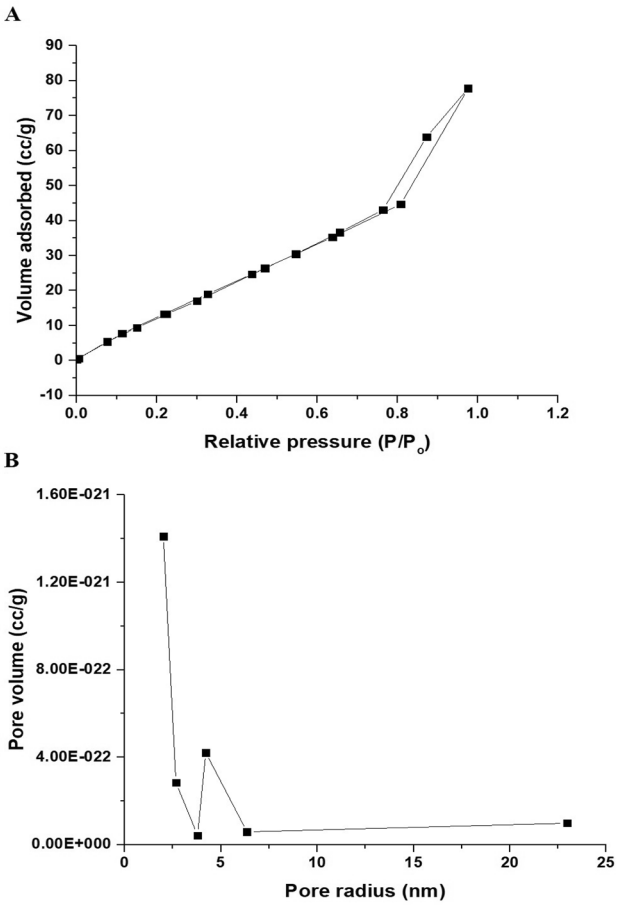

Fig. 5 The Nitrogen adsorption/desorption isotherm of $MgFe_2O_4$ nanoparticles (**A**). Pore size distribution curve (**B**)

The impact of the initial methylene blue dye solution pH shows a crucial function in every uptake procedure. It can influence both the charge on the surface of the adsorbent and the dye solution's chemistry. Figure 6 depicts the effect of initial methylene blue dye solution pH on the removal percentage of methylene blue dye using $MgFe_2O_4$ nanoparticles. The point of zero charge (pH_{PZC}) of the $MgFe_2O_4$ nanoparticles was determined as described by Khalifa et al. and found to be 6.58 [39]. The adsorption of methylene blue dye using $MgFe_2O_4$ nanoparticles increases rapidly as the pH increases from 2 to 8, where it attains equilibrium at pH 8 with a removal efficacy of 87.19%. The decreased uptake of methylene blue cationic dye at pH smaller than pH_{PZC} may be assigned to the abundant hydrogen ions (H^+) in the dye solution that compete with the methylene blue cationic dye for active positions on the $MgFe_2O_4$ surface, thereby hindering the uptake of methylene blue cationic dye. Furthermore, if the studied pH of the methylene blue dye solution is acidic, the functional groups that exist on the surface of $MgFe_2O_4$ become protonated. Hence, a positive charge creates on the surface of $MgFe_2O_4$

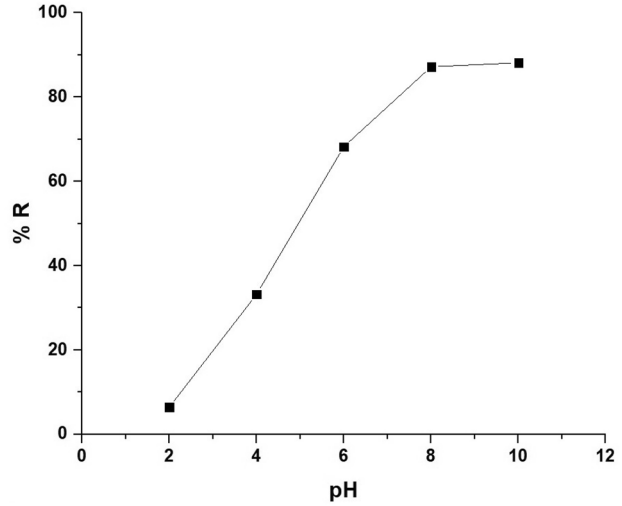

Fig. 6 The plot of methylene blue dye solution pH versus the removal percentage of methylene blue dye using $MgFe_2O_4$ nanoparticles

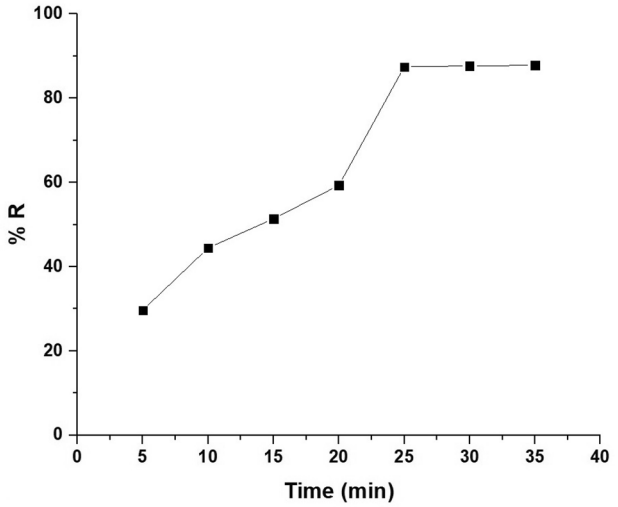

Fig. 7 The plot of ultrasonication time versus the removal percentage of methylene blue dye using $MgFe_2O_4$ nanoparticles

nanoparticles, resulting in weak adsorption for methylene blue dye. If the pH of the methylene blue dye solution is greater than pH_{PZC}, the deprotonation of functional groups rises the density of negative charges on the surface of $MgFe_2O_4$ nanoparticles. As methylene blue is a cationic dye, the negatively charged $MgFe_2O_4$ surface electrostatically attracts the methylene blue dye, which is positively charged [33]. Consequently, the optimum pH that achieves the maximum removal of methylene blue dye is 8.

3.2.2 Time Study

Figure 7 depicts the influence of the ultrasonication time on the uptake percentage of methylene blue dye using $MgFe_2O_4$ nanoparticles. The uptake of methylene blue dye using $MgFe_2O_4$ nanoparticles increases rapidly as the ultrasonication time increases from 5 to 25 min, where it reaches equilibrium at 25 min with a removal efficiency of 87.46%. Consequently, the optimum time that achieves the maximum removal of methylene blue dye is 25 min.

In order to assess the influence of ultrasounds on the methylene blue dye uptake procedure, uptake reactions were carried out using other typical mixing techniques such as shaking and stirring, as shown in Fig. 8 [40, 41]. The ultrasonication-assisted adsorption resulted in the highest removal percentage compared with shaking and stirring techniques. Hence, this confirms the methodology's superiority. In addition, the process of acoustic cavitation was responsible for the enhanced adsorption of methylene blue dye under the influence of ultrasound. The acoustic cavitation process includes the creation, development, and collapse of minute gas bubbles. Hence, this results in high energy amplitudes at a specific location. Cavitation induces convection in media by means of microjetting, microturbulence, microstreaming, and shock or acoustic waves. In addition, shock waves generate microscopic confusion within the interfacial coatings that edging adjacent solid particles, thereby accelerating the rate of mass transfer [31, 32]. Ultrasonication enhances the bulk transfer of methylene blue dye onto the $MgFe_2O_4$ surface via decreasing the resistance of diffusion. Thus, ultrasonication aids in achieving equilibrium in a shorter contact time than other conventional adsorption procedures [40–42].

The pseudo-first-order and pseudo-second-order kinetic models, were used to linearly fit the experimental data of the effect of time on methylene blue dye adsorption using

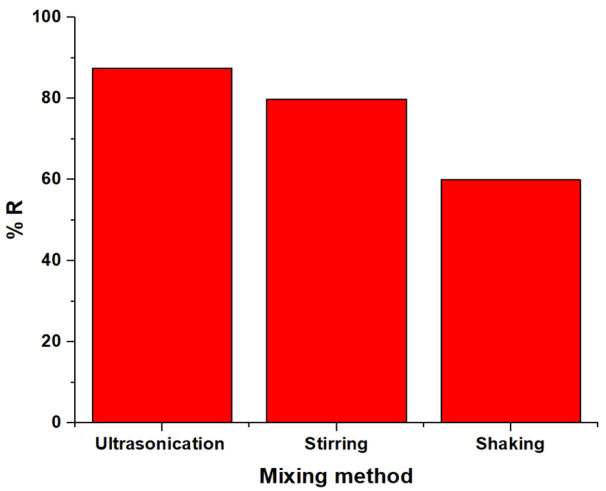

Fig. 8 The plot of removal percentage of methylene blue dye using $MgFe_2O_4$ nanoparticles versus some mixing methodologies

$MgFe_2O_4$ nanoparticles, as shown in Fig. 9A, B, respectively [33]. Table 1 presents the kinetic constants obtained from the linear fitting of experimental data. Majority of adsorption examinations over the last two decades utilized the pseudo-first-order and pseudo-second-order rate laws to model their kinetic datasets. The pseudo-first-order kinetic model assumes that physisorption limits the adsorption rate of the particles onto the adsorbent, while the pseudo-second-order model considers chemisorption as the rate-limiting mechanism of the process. In this work, the linear fitting of pseudo-second-order model produced the greatest correlation coefficient compared to pseudo-first-order. Moreover, the calculated adsorption capacity and experimental adsorption capacity (Q_{Exp}) values are closer to one another in the pseudo-second-order model than in the pseudo-first-order model. Consequently, the aforementioned observations suggest that the experimental data for the uptake of methylene blue dye by $MgFe_2O_4$ nanoparticles were described well with the pseudo-second-order kinetic model. Thus, the chemisorption process governs the ultrasonication-assisted adsorption of methylene blue dye onto $MgFe_2O_4$ nanoparticles.

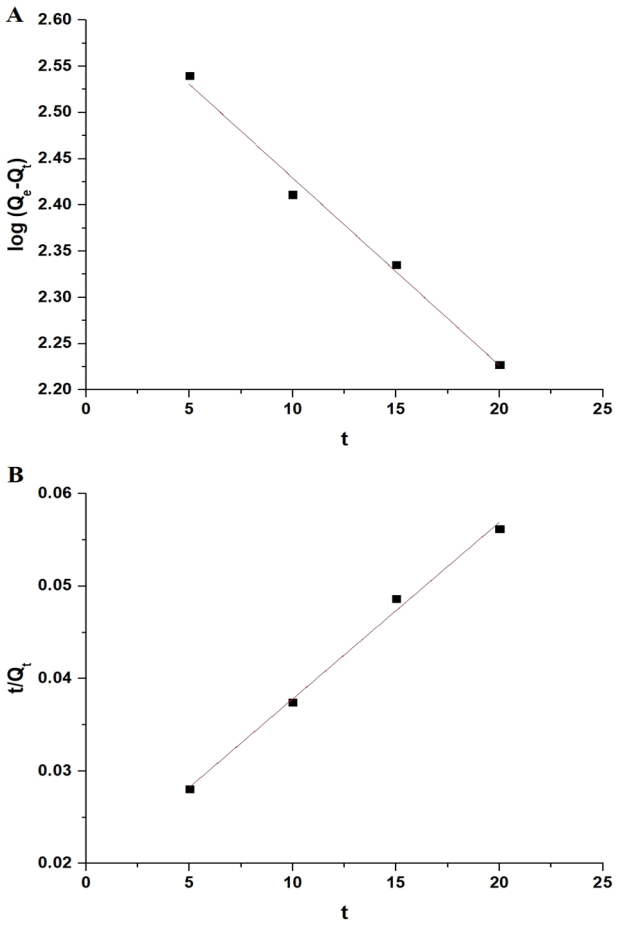

Fig. 9 Linear fitting of kinetic experimental data using the pseudo-first-order (**A**) and pseudo-second-order (**B**) models

3.2.3 $MgFe_2O_4$ Dose Study

According to the findings shown in Fig. 10, the methylene blue dye removal efficiency increases quickly as the $MgFe_2O_4$ dose increases from 0.0125 to 0.05 g, and then it nearly stabilizes at 0.05 g. Due to a rise in $MgFe_2O_4$ active sites with increasing $MgFe_2O_4$ dose, the methylene blue dye removal efficiency increased quickly. The small increase in methylene blue dye removal efficiency observed using 0.05 g of $MgFe_2O_4$ is caused by insufficient methylene blue dye molecules being adsorbed in the plentiful effective surface area offered by a greater $MgFe_2O_4$ quantity.

3.2.4 Initial Methylene Blue Dye Concentration Study

According to the findings shown in Fig. 11, the methylene blue dye removal efficiency decreases quickly as the concentration of methylene blue dye increases from 200 to 400 mg/L. The fact that at greater dye concentrations the effective positions on the surface of adsorbent become saturated and result in lower efficiency for removing the dye is the cause of the decrease in removal efficiency of methylene blue dye with rising initial methylene blue dye concentration.

The Langmuir and Freundlich equilibrium isotherms, were exploited to linearly fit the experimental data on methylene blue dye adsorption using $MgFe_2O_4$ nanoparticles, as shown in Fig. 12A, B, respectively [33]. Table 2 presents the equilibrium constants obtained from fitting experimental data. Majority of adsorption examinations over the last two decades utilized the Langmuir and Freundlich laws to model their equilibrium datasets. The Langmuir isotherm is applied to monolayer adsorption on homogeneous sites, whereas the Freundlich isotherm suites are applied to multilayer adsorption on heterogeneous sites. In this work, Langmuir isotherm fitting produced the highest correlation coefficient compared to Freundlich isotherm. Consequently, the experimental data for methylene blue dye adsorption onto $MgFe_2O_4$ nanoparticles fits well with the Langmuir isotherm and hence this indicates monolayer adsorption on homogeneous sites. Moreover, the

Table 1 The kinetic constants for the uptake of methylene blue dye onto $MgFe_2O_4$ nanoparticles

Q_{Exp} (mg/g)	Pseudo-second-order			Pseudo-second-order		
	k_1 (1/min)	Q (mg/g)	R^2	k_2 (g/mg.min)	Q (mg/g)	R^2
524.76	0.04668	428.41	0.9865	0.00019	523.56	0.9922

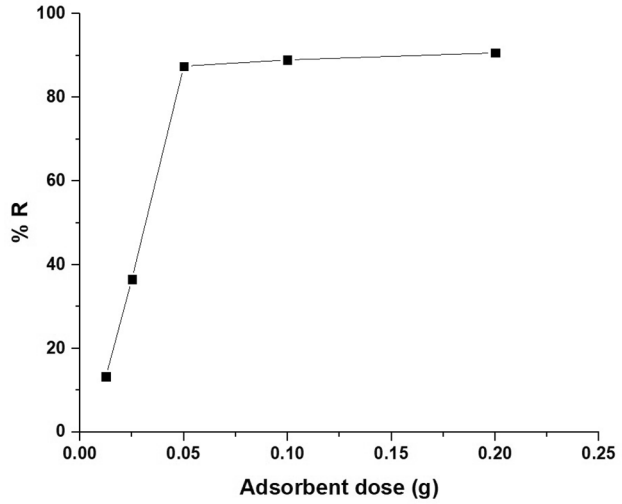

Fig. 10 The plot of adsorbent dose versus the removal percentage of methylene blue dye using $MgFe_2O_4$ nanoparticles

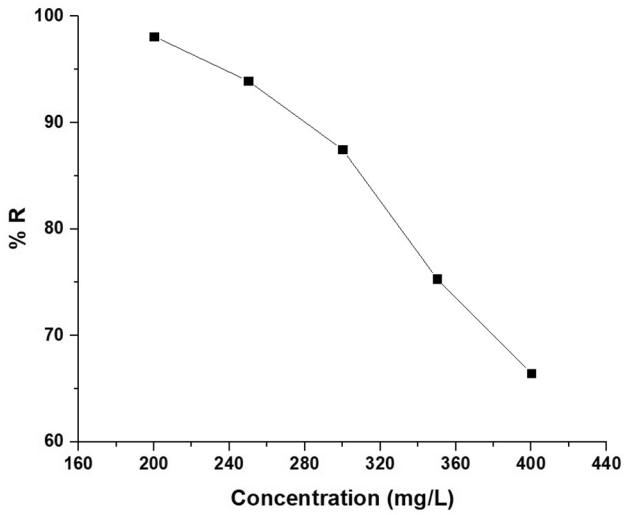

Fig. 11 The plot of initial methylene blue dye concentration versus the removal percentage of methylene blue dye using $MgFe_2O_4$ nanoparticles

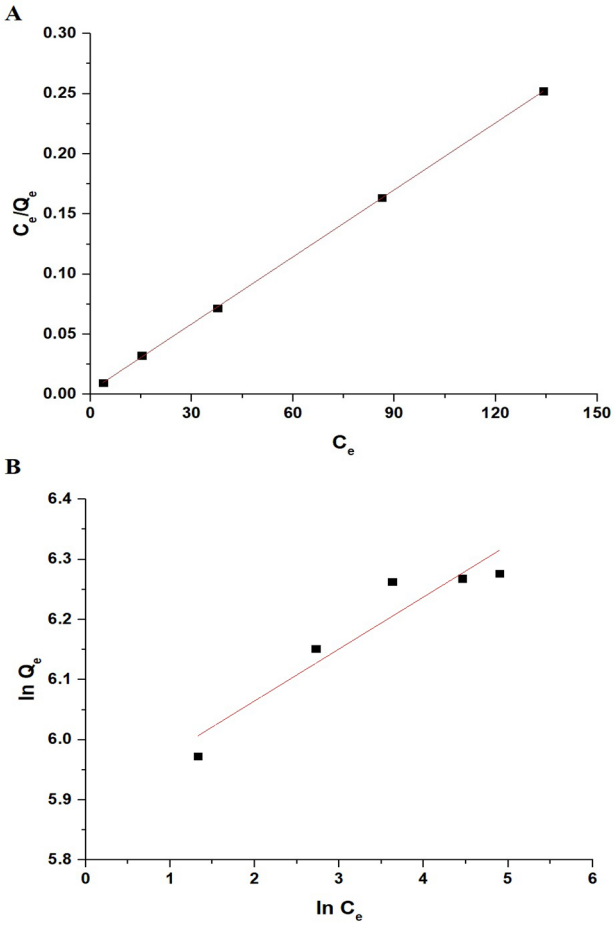

Fig. 12 Linear fitting of equilibrium experimental data using the Langmuir (**A**) and Freundlich (**B**) isotherms

Table 2 Equilibrium constants of methylene blue dye adsorption onto $MgFe_2O_4$ nanoparticles

Langmuir			Freundlich		
Q_{max} (mg/g)	K_L (L/mg)	R^2	Q_{max} (mg/g)	K_F (mg/g)(L/mg)$^{1/n}$	R^2
537.63	0.6327	0.9999	592.69	362.09	0.8679

maximum uptake capability of the $MgFe_2O_4$ nanoparticles toward methylene blue dye is 537.63 mg/g.

The uptake capability of the $MgFe_2O_4$ nanoparticles is higher than that of other adsorbents in the literature as shown in Table 3 [43–50].

3.2.5 Reusability Study

To investigate the reusability of $MgFe_2O_4$ nanoparticles, up to five consecutive adsorption cycles, the methylene blue dye-loaded $MgFe_2O_4$ nanoparticles were ignited at 500 °C for 2 h for the complete elimination of methylene blue dye. After that, at a solution pH of 8.0, adsorption experiments were conducted with 100 mL of 300 mg/L of methylene blue dye solution, 0.05 g of $MgFe_2O_4$ nanoparticles, and 25 min of ultrasonication. After the adsorption reaction, the $MgFe_2O_4$ nanoparticles were separated using an external magnetic field, washed with distilled water, dried at 120 °C for 2 h, and then ignited at 500 °C for the subsequent cycle. Figure 13 illustrates the change of methylene blue dye removal efficacy up to five sequential cycles. The results confirmed that there was little change in the removal percentage after five cycles. Hence, this demonstrates the

Table 3 Evaluation of the performance of $MgFe_2O_4$ nanoparticles for methylene blue dye removal relative to previously reported adsorbents

Adsorbent	Q (mg/g)	References
Amine functionalized sodium alginate hydrogel	400	[43]
Copolymer-type magnetic graphene oxide	170.3	[44]
Graphene oxide/mesoporous silica composite	416.67	[45]
Lignin-based activated carbon	493.28	[46]
Betaine-modified magnetic nanoparticles	136	[47]
Magnetic chitosan grafted with graphene oxide	81.5	[48]
Konjac glucomannan/graphene oxide hydrogel	133.6	[49]
Bi_2WO_6 microcrystals	60.2	[50]
$MgFe_2O_4$ nanoparticles	537.63	This study

excellent reusability of $MgFe_2O_4$ nanoparticles for the adsorption of methylene blue dye. Also, the stability of the regenerated $MgFe_2O_4$ nanoparticles was studied by carrying out the XRD analysis for the regenerated adsorbent (Figures omitted for brevity). The results confirmed that there is no difference in the positions of the XRD peaks or their intensities.

3.2.6 Effect of Co-existing Inorganic Materials

In order to prove the applicability of the process in real conditions, the influence of some anions and cations on the removal efficiency of methylene blue dye by the existing procedure was studied. The possible co-existing ion was introduced at several concentrations to a 100 mL of 300 µg/L methylene blue dye solution. The removal technique was carried out accurately as illustrated earlier in the effect of time, and its effectiveness was determined. The tolerance limit was recognized as the greatest concentration of the co-existing ion that resulted in a 5 percent removal error. Table 4 clearly illustrates that the majority of coexisting ions have a rather great tolerance limit, revealing the selectivity of the method. Therefore, the method can be applied in real conditions.

3.3 Mechanism of Adsorption of Methylene Blue Dye onto the $MgFe_2O_4$ Nanoparticles

FT-IR analysis was performed for the $MgFe_2O_4$ nanoparticles after the adsorption of methylene blue dye as shown in Fig. 14. The FT-IR spectrum of $MgFe_2O_4$ nanoparticles exhibits band at 3453 cm^{-1} due to the stretching vibration of O–H as shown in Fig. 3. After adsorption of methylene blue dye onto $MgFe_2O_4$ nanoparticles, the O–H group of $MgFe_2O_4$ nanoparticles interacts with the lone-pair electrons of NH_2 groups of methylene blue dye via hydrogen bonds, which is confirmed by the slight shifting of the O–H stretching vibration band to 3380 cm^{-1} as shown in Fig. 14. In addition, the new band at 1658 cm^{-1} in the spectrum of $MgFe_2O_4$ nanoparticles indicated the formation of ionic interactions between the cationic methylene blue dye and the negatively charged $MgFe_2O_4$ surface. Two bands that appear at 2855 and 3000 cm^{-1} are due to the stretching vibration of $-CH_3$ methyl and −H-aromatic groups of methylene blue dye. The spectra ranging from 1566 to 1362 cm^{-1}, are attributed to the stretching vibrations of

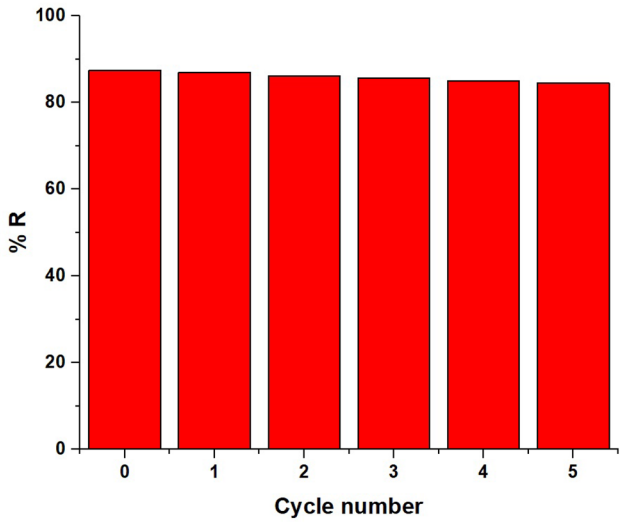

Fig. 13 Reusability study of $MgFe_2O_4$ nanoparticles for the removal of methylene blue dye up to five sequential cycles

Table 4 Effect of co-existing ions on the removal of methylene blue dye

Diverse ion	Tolerance limit (mg/L)
K^+	600
Na^+	600
Ca^{2+}	70
Mg^{2+}	70
Ba^{2+}	50
Cd^{2+}	50
Hg^{2+}	60
Cu^{2+}	50
Zn^{2+}	60
Ni^{2+}	50
Fe^{3+}	50
HCO^{3-}	1000
NO^{3-}	1000
Cl^-	800
SO_4^{2-}	1000

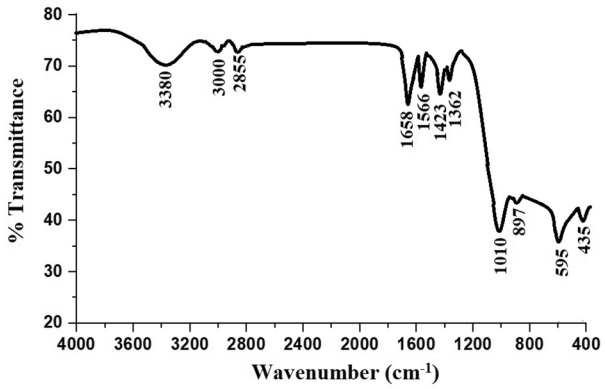

Fig. 14 The FT-IR spectrum of the $MgFe_2O_4$ nanoparticles after the adsorption of methylene blue dye

C = C aromatic of methylene blue dye. The bands at 897 and 1010 cm^{-1} are due to the aryl CH wagging vibration of methylene blue dye. Following the effect of pH, the results indicates that the electrostatic attraction controls the adsorption of methylene blue dye mechanism onto the $MgFe_2O_4$ sorbent. Hence, the adsorption of methylene blue dye mechanism is associated with the electrostatic attractions and hydrogen bond between the O–H group of $MgFe_2O_4$ nanoparticles and the NH_2 groups of methylene blue dye, as indicated by the pH and FTIR studies [51, 52].

4 Conclusion

$MgFe_2O_4$ nanoparticles were synthesized by the pechini sol gel method as an efficient adsorbent for the removal of methylene blue dye from aqueous media under ultrasonication. The ultrasonication aids in achieving equilibrium in a shorter contact time than other conventional adsorption procedures such as stirring and shaking due to the enhanced mass transfer. The maximum adsorption capacity of $MgFe_2O_4$ nanoparticles toward methylene blue dye is 537.63 mg/g. Adsorption of methylene blue dye using $MgFe_2O_4$ nanoparticles fits well with the Langmuir equilibrium isotherm as well as the pseudo-second-order kinetic model.

Acknowledgements The authors are grateful to Princess Nourah bint Abdulrahman University, Riyadh, Saudi Arabia for funding this work through Researchers Supporting Project number (PNURSP2023R35).

Author Contributions ASA (Experimental work- Research writing—Research review), FKA (Experimental Work-Writing the introduction-Preparing figures and tables), FAS (Preparing figures and tables), EAA (Idea, Experimental work, Research Writing). All authors reviewed the manuscript.

Funding This research was funded by Princess Nourah bint Abdulrahman University Researchers Supporting Project number (PNURSP2023R35), Princess Nourah bint Abdulrahman University, Riyadh, Saudi Arabia.

Declarations

Conflict of interest The authors confirm that there is no conflict of interest for this paper.

References

1. A. Kausar, S.T. Zohra, S. Ijaz, M. Iqbal, J. Iqbal, I. Bibi, S. Nouren, N. El, Messaoudi, A. Nazir, Int. J. Biol. Macromol. **224**, 1337 (2023)
2. S.K. Bhagat, K.E. Pilario, O.E. Babalola, T. Tiyasha, M. Yaqub, C.E. Onu, K. Pyrgaki, M.W. Falah, A.H. Jawad, D.A. Yaseen, N. Barka, Z.M. Yaseen, J. Clean. Prod. **385**, 135522 (2023)
3. G. Sriram, A. Bendre, E. Mariappan, T. Altalhi, M. Kigga, Y.C. Ching, H.Y. Jung, B. Bhaduri, M. Kurkuri, Sustain. Mater. Technol. **31**, e00378 (2022)
4. S. Sankar Sana, R. Haldhar, J. Parameswaranpillai, M. Chavali, S.C. Kim, Clean. Mater. **6**, 100161 (2022)
5. N. Aramesh, A.R. Bagheri, M. Bilal, Int. J. Biol. Macromol. **183**, 399 (2021)
6. A. Asfaram, M. Ghaedi, S. Agarwal, I. Tyagi, V.K. Gupta, RSC Adv. **5**, 18438 (2015)
7. M. Akrami, S. Danesh, M. Eftekhari, J. Inorg. Organomet. Polym. Mater. **29**, 1785 (2019)
8. E. Ghiasi, A. Malekzadeh, J. Inorg. Organomet. Polym. Mater. **30**, 2789 (2020)
9. X. Wang, J. Zhao, M. Le, H. Lin, J. Luan, G. Liu, X. Wang, J. Inorg. Organomet. Polym. Mater. **28**, 800 (2018)
10. A.M. Hameed, J. Inorg. Organomet. Polym. Mater. **30**, 2881 (2020)
11. S.K. Lakkaboyana, S. Khantong, N.K. Asmel, A. Yuzir, W.Z. Wan, Yaacob, J. Inorg. Organomet. Polym. Mater. **29**, 1658 (2019)
12. E.A. Abdelrahman, R.M. Hegazey, S.H. Ismail, H.H. El-Feky, A.M. Khedr, M. Khairy, A.M. Ammar, Arab. J. Chem. **15**, 104372 (2022)
13. R.M. Hegazey, E.A. Abdelrahman, Y.H. Kotp, A.M. Hameed, A. Subaihi, J. Mater. Res. Technol. **9**, 1652 (2020)
14. E.A. Abdelrahman, J. Mol. Liq. **253**, 72 (2018)
15. A.A. Moneer, N.M. El-Mallah, M.S. Ramadan, A.M. Shaker, Egypt. J. Aquat. Res. **48**, 191 (2022)
16. J.P. Dhal, M. Sethi, B.G. Mishra, G. Hota, Mater. Lett. **141**, 267 (2015)
17. S.K. Sahoo, G.K. Panigrahi, J.K. Sahoo, A.K. Pradhan, A.K. Purohit, J.P. Dhal, J. Mol. Liq. **326**, 115364 (2021)
18. S.K. Sahoo, G.K. Panigrahi, J.P. Dhal, J.K. Sahoo, A.K. Behera, P.C. Panda, P. Patel, S.K. Mund, S.M. Muduli, L. Panda, Colloids Surf. Physicochem. Eng. Asp. **652**, 129877 (2022)
19. J.P. Dhal, B.G. Mishra, G. Hota, J. Environ. Chem. Eng. **2**, 2188 (2014)
20. S.K. Sahoo, J.P. Dhal, G.K. Panigrahi, Compos. Commun. **22**, 100496 (2020)
21. J.P. Dhal, T. Dash, G. Hota, J. Porous Mater. **27**, 205 (2020)
22. J.P. Dhal, B.G. Mishra, G. Hota, Int. J. Environ. Sci. Technol. **12**, 1845 (2015)
23. H.F. Youssef, R.A. Nasr, E.A.A. El-Anwar, H.S. Mekky, S.H.A. El Rahim, Microporous Mesoporous Mater. **328**, 111485 (2021)
24. C. Nuanhchamnong, K. Kositkanawuth, N. Wantaneeyakul, Results Eng. **14**, 100451 (2022)

25. N. Vasiraja, R. Saravana Sathiya, Prabhahar, A. Joshua, J. Clean. Prod. **397**, 136579 (2023)
26. P. Das, A. Debnath, Water Pract. Technol. **16**, 1141 (2021)
27. M. Singh, H.S. Dosanjh, H. Singh, J. Water Process. Eng. **11**, 152 (2016)
28. P. Zhang, I. Lo, D. O'Connor, S. Pehkonen, H. Cheng, D. Hou, J. Colloid Interface Sci. **508**, 39 (2017)
29. L. Lu, J. Li, J. Yu, P. Song, D.H.L. Ng, Chem. Eng. J. **283**, 524 (2016)
30. L. Zhou, J. Liu, A. Lu, J. Shen, J. Xu, H. Jiang, Chem. Eng. J. **428**, 131174 (2022)
31. A. Ali, M. Bilal, R. Khan, R. Farooq, M. Siddique, Environ. Sci. Pollut. Res. **25**, 22920 (2018)
32. M. Saad, H. Tahir, J. Khan, U. Hameed, A. Saud, Ultrason. Sonochem. **34**, 600 (2017)
33. A.S. Al-Wasidi, A.M. Naglah, F.A. Saad, E.A. Abdelrahman, Arab. J. Chem. **15**, 104178 (2022)
34. E.A. Abdelrahman, E.S. Al-Farraj, Nanomaterials **12**, 3992 (2022)
35. A.S. Al-Wasidi, A.A. Almehizia, A.M. Naglah, H.M. Alkahtani, F.K. Algethami, E.S. Al-Farraj, M.T. Basha, E.A. Abdelrahman, Int. J. Environ. Anal. Chem. **00**, 1 (2022)
36. A.S. Al-Wasidi, F.A. Saad, A.M. Munshi, E.A. Abdelrahman, RSC Adv. **13**, 5656 (2023)
37. M. Ghanbarian, M. Ghanbarian, A.H. Mahvi, T. Tabatabaie, Int. J. Biol. Macromol. **148**, 574 (2020)
38. E.A. Abdelrahman, Y.G. Abou El-Reash, H.M. Youssef, Y.H. Kotp, R.M. Hegazey, J. Hazard. Mater. **401**, 123813 (2021)
39. M.E. Khalifa, E.A. Abdelrahman, M.M. Hassanien, W.A. Ibrahim, J. Inorg. Organomet. Polym. Mater. **30**, 2182 (2020)
40. T.R. Bastami, S. Khaknahad, M. Malekshahi, Environ. Sci. Pollut. Res. **27**, 9364 (2020)
41. M. Najafi, T.R. Bastami, N. Binesh, A. Ayati, S. Emamverdi, J. Ind. Eng. Chem. **116**, 489 (2022)
42. E. Omrani, A. Ahmadpour, M. Heravi, T.R. Bastami, J. Water Process. Eng. **47**, 102581 (2022)
43. C.B. Godiya, Y. Xiao, X. Lu, Int. J. Biol. Macromol. **144**, 671 (2020)
44. C. Bo, Z. Jia, B. Liu, X. Dai, G. Ma, Y. Li, J. Taiwan. Inst. Chem. Eng. **138**, 104499 (2022)
45. M. Sari Yilmaz, Microporous Mesoporous Mater. **330**, 111570 (2022)
46. Z. Liao, Y.H. Zhu, G.T. Sun, L. Qiu, M.Q. Zhu, Ind. Crops Prod. **175**, 114266 (2022)
47. H. Wang, S. Jia, H. Wang, B. Li, W. Liu, N. Li, J. Qiao, C.Z. Li, Sci. Bull. **62**, 319 (2017)
48. L. Fan, C. Luo, X. Li, F. Lu, H. Qiu, M. Sun, J. Hazard. Mater. **215–216**, 272 (2012)
49. L. Gan, S. Shang, E. Hu, C.W.M. Yuen, S.X. Jiang, Appl. Surf. Sci. **357**, 866 (2015)
50. D. Wang, J. Zhang, L. Guo, X. Dong, H. Shen, F. Fu, Mater. Res. Bull. **83**, 387 (2016)
51. A.S. Al, W. Maram, T.B. Reem, M.A. Eida, S. Al Farraj, E.A. Abdelrahman, J. Inorg. Organomet. Polym. Mater. (2023). https://doi.org/10.1007/s10904-023-02554-7
52. M.G. Ghoniem, F.A.M. Ali, B.Y. Abdulkhair, M.R.A. Elamin, A.M. Alqahtani, S. Rahali, M.A. Ben Aissa, Nanomaterials **12**, 1 (2022)